PAPER

Simple beam hardening correction method (2DCalBH) based on 2D linearization

IOP Publishing Phys. Med. Biol. 67 (2022) 115005 https://doi.org/10.1088/1361-6560/ac5f71

Physics in Medicine & Biology

IPEM Institute of Physics and Engineering in Medicine

RECEIVED
18 November 2021

REVISED
8 March 2022

ACCEPTED FOR PUBLICATION
21 March 2022

PUBLISHED
19 May 2022

PAPER

Simple beam hardening correction method (2DCalBH) based on 2D linearization

Cristobal Martinez[1,2], **Jeffrey A Fessler**[3], **Manuel Desco**[1,2,4,5,*] **and Monica Abella**[1,2,4,*]

[1] Dept. Bioingeniería e Ingeniería Aeroespacial, Universidad Carlos III de Madrid, Spain
[2] Instituto de Investigación Sanitaria Gregorio Marañón, Madrid, Spain
[3] Electrical Engineering and Computer Science department, The University of Michigan, Ann Arbor, United States of America
[4] Centro Nacional de Investigaciones Cardiovasculares Carlos III (CNIC), Madrid, Spain
[5] Centro de investigación en red en salud mental (CIBERSAM), Madrid, Spain
[*] Authors to whom any correspondence should be addressed.

E-mail: desco@hggm.es **and** mabella@ing.uc3m.es

Keywords: beam hardening, CT, polychromatic, cupping, calibration, artifact

Supplementary material for this article is available online

Abstract

Objective. The polychromatic nature of the x-ray spectrum in computed tomography leads to two types of artifacts in the reconstructed image: cupping in homogeneous areas and dark bands between dense parts, such as bones. This fact, together with the energy dependence of the mass attenuation coefficients of the tissues, results in erroneous values in the reconstructed image. Many post-processing correction schemes previously proposed require either knowledge of the x-ray spectrum or the heuristic selection of some parameters that have been shown to be suboptimal for correcting different slices in heterogeneous studies. In this study, we propose and validate a method to correct the beam hardening artifacts that avoids such restrictions and restores the quantitative character of the image. *Approach*. Our approach extends the idea of the water-linearization method. It uses a simple calibration phantom to characterize the attenuation for different soft tissue and bone combinations of the x-ray source polychromatic beam. The correction is based on the bone thickness traversed, obtained from a preliminary reconstruction. We evaluate the proposed method with simulations and real data using a phantom composed of PMMA and aluminum 6082 as materials equivalent to water and bone. *Main results*. Evaluation with simulated data showed a correction of the artifacts and a recovery of monochromatic values similar to that of the post-processing techniques used for comparison, while it outperformed them on real data. *Significance*. The proposed method corrects beam hardening artifacts and restores monochromatic attenuation values with no need of spectrum knowledge or heuristic parameter tuning, based on the previous acquisition of a very simple calibration phantom.

1. Introduction

X-ray computed tomography (CT) can characterize attenuation coefficients of the patient tissues, which are roughly decreasing functions of energy in the usual range of energies used in clinical and preclinical scenarios (from 30 to 150 keV). Commercial scanners use polychromatic sources because no x-ray lasers exist as a usable alternative. Since the attenuation coefficients are higher for lower energies, low-energy photons are preferentially absorbed, thus increasing the effective energy of the spectrum; this effect is known as beam hardening. Classical reconstruction methods assume a monochromatic source and do not take into account the polychromatic nature of the spectrum, producing two artifacts in the reconstructed image that hinder quantitative values: (1) cupping in large homogeneous areas and (2) dark bands between dense objects such as bone (Brooks and Di Chiro 1976).

The simplest correction method, implemented in most commercial scanners, is the water linearization (Brooks and Di Chiro 1976, Herman 1979), which assumes that the object in the scan field is composed of only water. This assumption compensates the cupping artifact but produces a suboptimal correction of the dark bands in heterogeneous objects. The method is based on a linearization function that replaces the energy-dependent attenuation values, given by the so-called beam hardening function, F_{BH}, with the corresponding monochromatic attenuation values, given by F_{MONO}. Considering the Beer–Lambert law, one can model F_{MONO} for each thickness traversed, t, as:

$$F_{\mathrm{MONO}}(t) = \ln\left(\frac{I_0}{I}\right) = \int \mu(\varepsilon_0)\,dt = \mu(\varepsilon_0)t, \tag{1}$$

where I_0 is the incident intensity, I is the transmitted intensity, ε_0 is a specific energy value and μ is the attenuation coefficient of the traversed material. In contrast, F_{BH} adds the energy dependence to equation (1):

$$F_{\mathrm{BH}}(t) = \ln\left(\frac{I_0}{I}\right) = \ln\left[\frac{\int I_0(\varepsilon)\,d\varepsilon}{\int I_0(\varepsilon)e^{-\mu(\varepsilon)t}d\varepsilon}\right], \tag{2}$$

where ε spans the range of energies of the polychromatic spectrum. One can obtain F_{BH} experimentally by a calibration step with a phantom made of soft-tissue equivalent material. Then, as there is no beam-hardening effect when the amount of tissue traversed is zero (Herman 1979), $F_{\mathrm{MONO}}(t)$ can be calculated as the derivative of F_{BH} at 0.

To correct both cupping and dark bands, the sample often is modeled as composed of soft tissue and bone, since most tissues behave like water and only bone is significantly different (Elbakri and Fessler 2003). Previously proposed correction methods based on post-processing estimate the bone and soft-tissue thicknesses traversed from an initial reconstruction and calculate a correction factor that depends on those thicknesses. Nalcioglu and Lou (1979) analytically obtained the equivalent monochromatic attenuation at the effective energy for each thickness of soft tissue and bone, F_{MONO}, from the knowledge of the spectrum and the mass attenuation coefficients of these tissues. Joseph *et al* (1978) corrected for cupping using water linearization and included a compensation for dark bands based on the concept of 'effective density', which is the amount of water that would produce the same beam-hardening effect as the given amount of bone traversed. The main drawback is that the characterization of this effective density needs the knowledge of the spectrum, which is not always available. To avoid the need of this information, the effective density can be approximated by a second-order polynomial, the coefficients of which can be optimized by visual inspection or otherwise, as in Abella *et al* (2020). This approach will be referred to as $\mathrm{JS}_{\mathrm{pol}}$ from here on.

Other works proposed a correction based on a linear combination of uncorrected and overcorrected images, where coefficients are found through the iterative minimization of the image flatness (Kyriakou *et al* 2010) (EBHC) or the entropy (Schuller *et al* 2015) (sfEBHC). However, the former method has been shown to not completely correct the dark bands (Jin *et al* 2015) while the latter method showed overcompensation for the dark bands in real studies (Schuller *et al* 2015). Recently, in the industrial field, two different methods proposed to use epipolar consistency conditions to reduce beam hardening artifacts (Würfl *et al* 2019, Würfl 2020). However, these methods produce a change in the soft-tissue texture and the authors are unsure about its performance in clinical CT.

Alternatively, iterative reconstruction methods can incorporate a model of the beam-hardening effect into the forward model to correct the beam-hardening artifacts (Yan *et al* 2000, De Man *et al* 2001, Elbakri and Fessler 2002, Abella *et al* 2020). These methods also provide robustness to noise, making them suitable for low-dose acquisitions, but their high computational cost imposes an undesirably high burden for standard SNR acquisitions.

We present a new post-processing method (2DCalBH) based on the extension of the water-linearization method to consider two tissue types, i.e. both soft tissue and bone. The beam-hardening and monochromatic functions are estimated by scanning a simple calibration phantom made up of soft-tissue and bone equivalent materials. This strategy overcomes the main drawbacks of previous methods, which rely either on the knowledge of the spectrum or on a polynomial model for the beam-hardening effect with coefficients that have been shown not to completely compensate the dark bands (Jin *et al* 2015, Schuller *et al* 2015). Preliminary results were presented in an earlier conference paper (Martínez *et al* 2016) based on simulated data using an ideal calibration phantom composed of soft tissue and bone. The present work extends the experiments on simulated data and evaluates the method on real data with a realistic calibration phantom made of an aluminum alloy and PMMA as materials equivalent to bone and soft tissue.

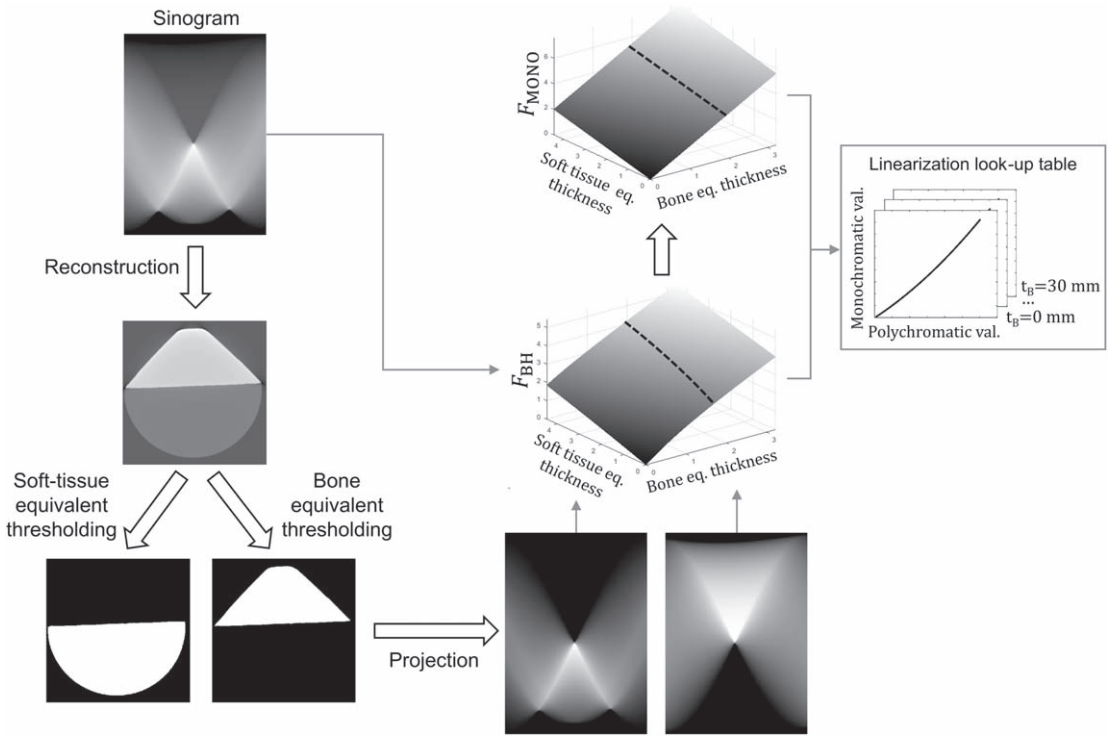

Figure 1. Workflow of the calibration (example for one slice).

2. Materials and methods

Following previous post-processing methods, we consider the sample to be composed of two tissue types: bone (B) and soft tissue (ST). Under this assumption, equations (1) and (2) can be rewritten as:

$$F_{\mathrm{MONO}}(t_{\mathrm{B}}, t_{\mathrm{ST}}) = \mu_{\mathrm{B}}(\varepsilon_0)t_{\mathrm{B}} + \mu_{\mathrm{ST}}(\varepsilon_0)t_{\mathrm{ST}}, \tag{3}$$

$$F_{\mathrm{BH}}(t_{\mathrm{B}}, t_{\mathrm{ST}}) = \ln\left[\frac{\int I_0(\varepsilon)d\varepsilon}{\int I_0(\varepsilon)e^{-(\mu_{\mathrm{B}}(\varepsilon)t_{\mathrm{B}}+\mu_{\mathrm{ST}}(\varepsilon)t_{\mathrm{ST}})}d\varepsilon}\right], \tag{4}$$

where $\mu_{\mathrm{ST}}(\varepsilon_0)$ and $\mu_{\mathrm{B}}(\varepsilon_0)$ represent the attenuation coefficients of soft tissue and bone at the effective energy of the spectrum, ε_0.

Figure 1 shows the calibration workflow for obtaining $F_{\mathrm{BH}}(t_{\mathrm{B}}, t_{\mathrm{ST}})$ and $F_{\mathrm{MONO}}(t_{\mathrm{B}}, t_{\mathrm{ST}})$ experimentally from a scan of a phantom composed of bone and soft-tissue equivalent materials. Each material is segmented in a preliminary reconstruction and then projected to obtain the bone and soft-tissue thicknesses, $(t_{\mathrm{B}}, t_{\mathrm{ST}})$ for each projection value, $F_{\mathrm{BH}}(t_{\mathrm{B}}, t_{\mathrm{ST}})$. Typically, the $F_{\mathrm{BH}}(t_{\mathrm{B}}, t_{\mathrm{ST}})$ function is fitted with a polynomial function (Alvarez and Macovski 1976), which could lead to non-monotonically increasing values. To ensure monotonicity, we fit the $F_{\mathrm{BH}}(t_{\mathrm{B}}, t_{\mathrm{ST}})$ generated to a logarithmic function:

$$\begin{aligned} &F_{\mathrm{BH}}(t_{\mathrm{B}}, t_{\mathrm{ST}}) \\ &= -\ln\left(a \times e^{-(b\times t_{\mathrm{ST}}+c\times t_{\mathrm{B}})} + (1-a) \times e^{-(d\times t_{\mathrm{ST}}+f\times t_{\mathrm{B}})}\right), \end{aligned} \tag{5}$$

where a, b, c, d, e and f are the fitting coefficients obtained with non-linear least squares method, initialized with values drawn from a uniform random distribution between 0 and 1. Slope values $\mu_{\mathrm{ST}}(\varepsilon_0)$ and $\mu_{\mathrm{B}}(\varepsilon_0)$ in equation (3) are estimated as the partial derivatives of the beam-hardening function at the (0, 0) point, i.e. $\frac{\partial F_{\mathrm{BH}}(0,0)}{\partial t_{\mathrm{Bone}}}$ and $\frac{\partial F_{\mathrm{BH}}(0,0)}{\partial t_{\mathrm{ST}}}$.

Ideally, the correction would be obtained with a linearization function that replaces the energy-dependent attenuation values, $F_{\mathrm{BH}}(t_{\mathrm{B}}, t_{\mathrm{ST}})$, with the corresponding monochromatic attenuation values, $F_{\mathrm{MONO}}(t_{\mathrm{B}}, t_{\mathrm{ST}})$. However, $F_{\mathrm{BH}}(t_{\mathrm{B}}, t_{\mathrm{ST}})$ is not injective, i.e. there are multiple combinations of $(t_{\mathrm{B}}, t_{\mathrm{ST}})$ that result in the same value. To solve this non-uniqueness, we use the bone thickness, $\hat{t}_B$, as a table index parameter and generate multiple water-linearization functions from the pairs $F_{\mathrm{BH}}(\hat{t}_B, t_{\mathrm{ST}}) - F_{\mathrm{MONO}}(\hat{t}_B, t_{\mathrm{ST}})$ (see dashed lines in figure 1). These water-linearization functions are fitted by second-order polynomial regressions, using linear least squares, and the coefficients are stored in a look-up table (LUT) for each $\hat{t}_B$ value. A bone-thickness spacing

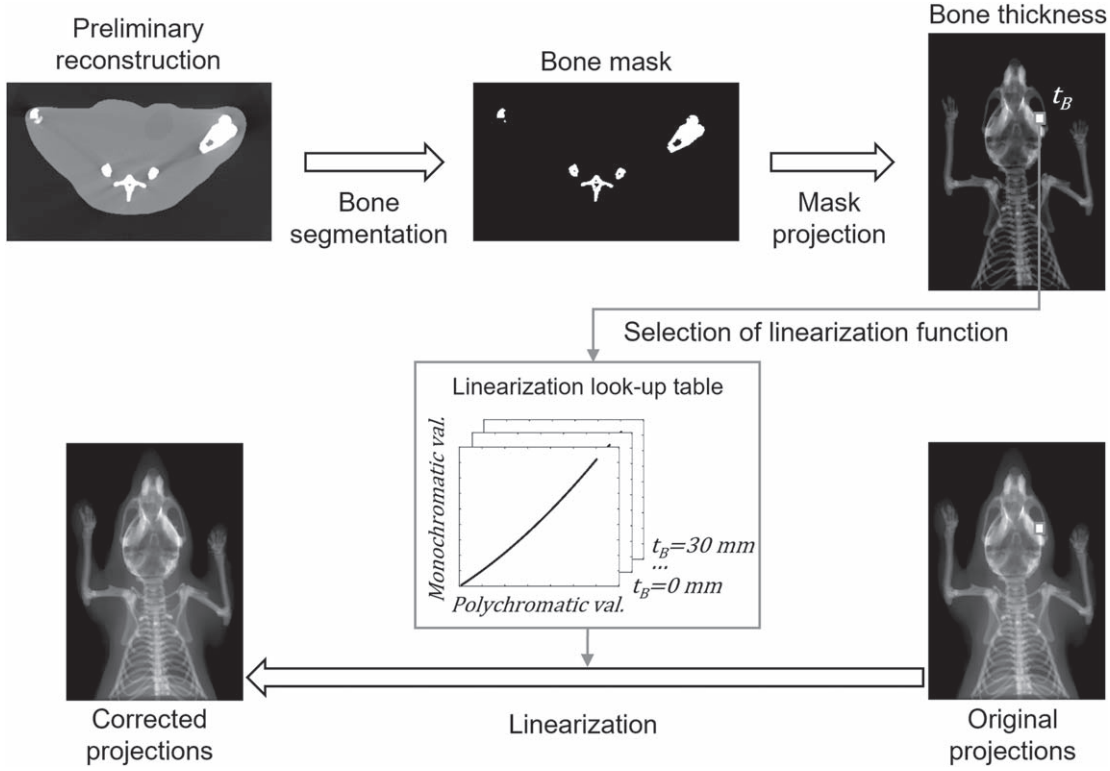

Figure 2. Workflow of the proposed correction method.

in the LUT (sampling of $\hat{t}_B$) below the voxel size prevents streak artifacts from a wrong selection of the linearization function.

Figure 2 shows the workflow of the proposed correction method. The bone is segmented by thresholding from a preliminary reconstruction and projected to obtain the bone thickness $\hat{t}_B$ corresponding to each pixel in the projection. This bone thickness, interpolated by nearest neighbor method, is used to select the appropriate coefficients of the linearization function from the LUT, which will be applied to that pixel. tables 1 and 2 show the pseudo-code of the method (*fitLog* refers to equation (5)).

2.1. Tissue equivalent materials

A realistic calibration phantom can be made up of PMMA as an equivalent of soft-tissue and aluminum 6082 (AL6082) for bone, as proposed in Martinez *et al* (2020). While PMMA is a good substitute for soft tissue in terms of beam hardening, AL6082 does not match bone very well in this regard. The deviation is due to the difference in density between cortical bone (1.92 g cm^{-3}) and AL6082 (2.7 g cm^{-3}), which can be compensated by multiplying the bone thickness by a weighting factor equal to the ratio of densities, 2.7/1.92 (clarifying plots can be found in supplementary data available online at stacks.iop.org/PMB/67/115005/mmedia).

3. Evaluation methods

The proposed method, 2DCalBH, was evaluated using simulations and real data by comparing with $JS_{pol,}$ the polynomial approximation of Joseph and Spital (1978) suggested in Abella *et al* (2020), and with EBHC (Kyriakou *et al* 2010) and sfEBHC (Schuller *et al* 2015). Simulations emulated a preclinical scanner at source voltages of 40 and 50 kVp. Real data were acquired in a small-animal scanner at source voltages of 40 and 50 kVp.

Comparisons with simulated data were performed in terms of visual inspection and root-mean-square error (RMSE) with respect to the monochromatic reconstruction. Comparisons with real data were assessed only by visual inspection since there was no ground truth available in this case.

3.1. Evaluation on simulated data

The evaluation on simulated preclinical data used a 2D phantom made up of a soft tissue ellipse (1 g cm^{-3}) with major axis of 6 cm and minor axis of 4.8 cm, one ellipsoid of fat (0.9 g cm^{-3}) with major axis of 4 cm and minor axis of 3.2 cm, ten bone inserts (1.92 g cm^{-3}) with diameters from 0.48 to 0.32 cm, and two air circles (0 g cm^{-3}).

Table 1. Pseudocode of 2DCalBH calibration.

```
procedure calibration (PhantomProjs)
1: PhantomVolume = recontruction (PhantomProjs)
2: BoneMask = segmentBone(PhantomVolume)
3: SoftTissueMask = segmentSoftTissue(PhantomVolume)
4: SoftTissueThickness = project(SoftTissueMask)
5: BoneThickness = project(BoneMask)
6: bh_funct = fitLog(SoftTissueThickness,BoneThickness, PhantomProjs)
7: monocromatic_funct = fitPlane(deriv_x(bh_funct(0,0)),
     deriv_y(bh_funct(0,0)))
8: for b = 1 to max(BoneThickness)
9:   LUT(b) = fitQuadratic(bh_funct(:,b), monochromatic_funct (:,b))
10:end
```

Table 2. Pseudocode of 2DCalBH correction.

```
procedure BHcorrection (LUT, SampleProjs)
1: SampleVolume=reconstruction(SampleProjs)
2: BoneMask=segmentBone(SampleVolume)
3: BoneThickness=project(BoneMask)
4: for pix=1 to NumberOfPixels
5:   LinearizationCoefs=LUT(BoneThinckness(pix))
7:   CorrectedProjs(pix)=applyQuadratic(LinearizationCoefs,
       SampleProjs(pix))
8: end
```

Mass attenuation coefficient and densities for those materials were obtained from the National Institute of Standards and Technology (Hubbell and Seltzer 1995). Projection data were simulated with the MIRT toolbox (https://github.com/JeffFessler/mirt), based on parallel-beam geometry, generating 180 projections within a 180-degree angular span. We did not simulate scatter and the blank scan value (detector measurement with no sample) was 10^6 counts per detector element. Two different polychromatic spectra were simulated: 40 and 50 kVp, with 2.5 mm of aluminum filtration. Equivalent monochromatic sources were simulated at the corresponding effective energies: 28.5 and 33.1 keV for the 40 kVp and 50 kVp polychromatic spectrum, respectively. Figure 3 shows the reconstructed images of the evaluation phantom from simulated data using these four spectra. Two extra experiments based on a phantom similar to the one used by Kyriakou *et al* (2010) (EBHC) and by Schuller *et al* (2015) (sfEBHC) but adapted to a small-animal scanner can be found in the supplementary data.

3.2. Evaluation on real data

Evaluation with real data was based on three rodent studies (figure 4), head and abdomen of a rat, and a whole mouse with an intraperitoneal administration of the contrast agent iopamiro® (iopamidol), acquired with the CT subsystem of ARGUS PET/CT (SEDECAL) (Vaquero *et al* 2008). Acquisition parameters were 40 kVp and 50 kVp with a current of 340 μA and 200 μA, respectively, for the head and abdomen studies, and 40 kVp with a current of 340 μA for the mouse study. We obtained 360 projections of 514 $\times$ 574 pixels with a pixel size of 0.2 mm over a 360-degree angular span. Reconstructions were done with the FUX-Sim toolbox (Abella *et al* 2017), which includes an FDK-based algorithm (Feldkamp *et al* 1984), resulting in volumes of 514 $\times$ 514 $\times$ 574 voxels with a voxel size of 0.121 mm^3. Results on two extra rodent studies can be found in the supplementary data.

3.3. Implementation of the methods

The calibration needed for the water linearization (Herman 1979) was generated following two different approaches: (1) a digital phantom composed of soft tissue (ideal) used for simulations; and (2) digital and true phantoms composed of PMMA (realistic) for simulations and real data (figure 5, top row). The linearization function obtained was fitted to a second-order polynomial (Herman 1979).

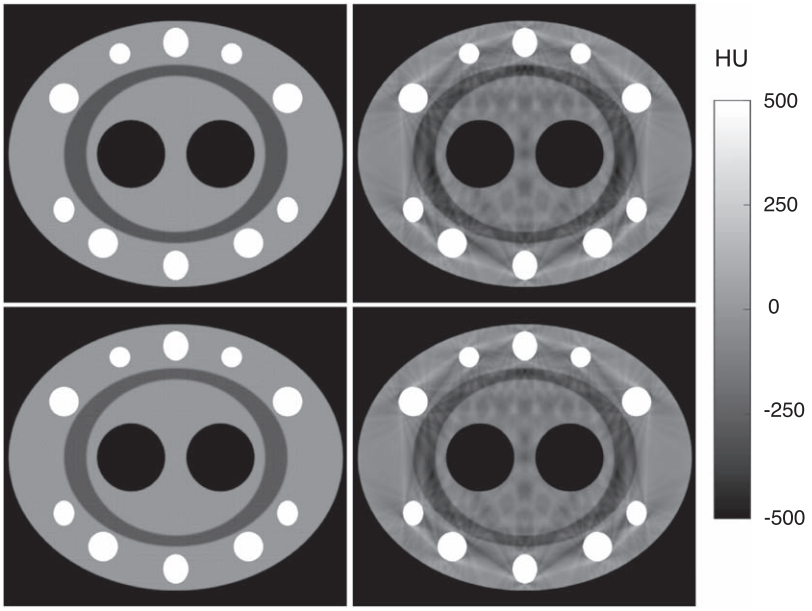

Figure 3. Evaluation phantom using monochromatic (left column) and polychromatic (right column) simulations at 40 kVp (top row) and 50 kVp (bottom row), reconstructed using the FBP algorithm.

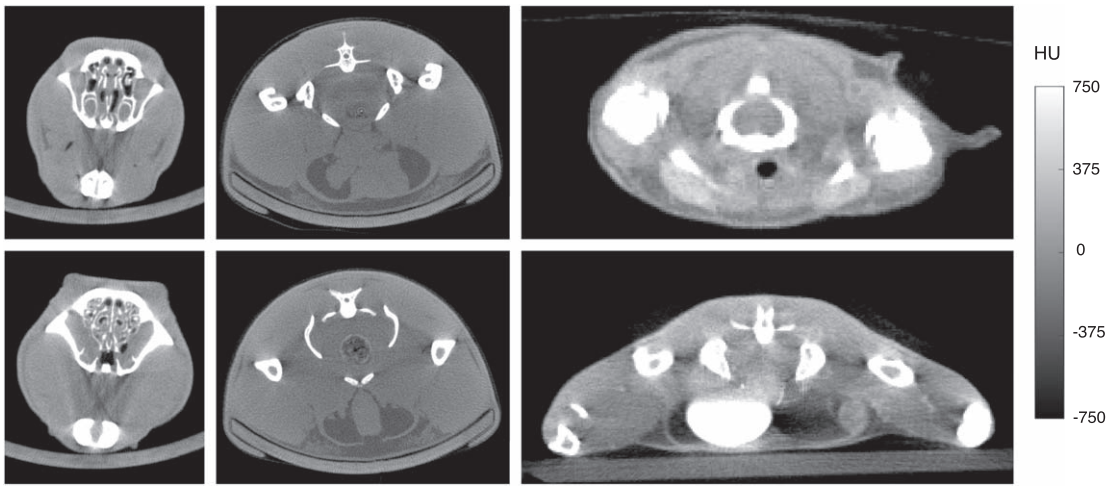

Figure 4. Axial slices used to optimize the JS_{pol} coefficients (top row) and a second slice of the same study (bottom row) for the rat head (left column) and abdomen (center column) studies at 50 kVp and the contrast-enhanced mouse study (right column) at 40 kVp, reconstructed using the FDK algorithm.

We implemented JS_{pol} according to the following equation:

$$\text{projection}_{\text{JSpol}} = \text{projection}_{\text{W}} + At_{\text{B}} + Bt_{\text{B}}^2\,, \tag{6}$$

where $\text{projection}_{\text{JSpol}}$ is the JS_{pol}-corrected data, $\text{projection}_{\text{W}}$ is the water-corrected data, t_B is the bone thickness obtained from a preliminary reconstruction, A is the parameter to recover the monochromatic bone values and B is the parameter that controls the dark-band correction. We selected A and B to minimize the RMSE with respect to monochromatic values in simulated data. For real data, we heuristically chose a different set of parameters for each type of study as those that best reduced the dark bands in a visual inspection of a representative axial slice. Selected slices for each study are shown in the top row of figure 4. Table 3 shows the JS_{pol} parameters selected.

EBHC and sfEBHC started with an initial reconstruction corrected by water linearization.

In EBHC, bone segmentation was based on a soft-threshold where the voxels above 500 HU were assumed to be bone, while the values between 500 HU and 100 HU were assumed to be a mixture of bone and soft tissue and estimated with a linear weighting function with weights between 0 and 1 (all values extracted from

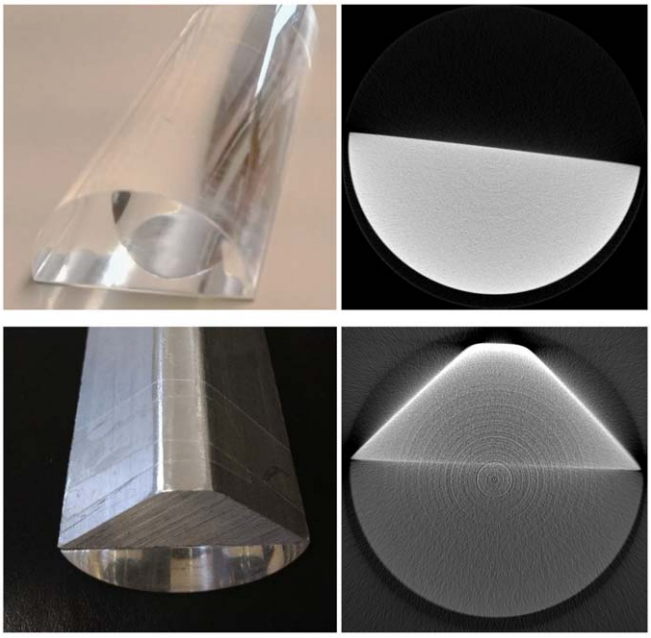

Figure 5. Photograph (left column) and axial view of the CT reconstruction (right column) of the calibration phantoms used for the water linearization, made of PMMA, (top row) and for 2DCalBH, made up of PMMA and AL6082 (bottom row).

Table 3. JS_{pol} parameters for simulations and real data.

Parameter	Simulation		Real data	
	40 kVp	50 kVp	40 kVp	50 kVp
A	0.5	0.41	0.1	0.1
B	0.26	0.22	0.8	0.73

Kyriakou *et al* (2010)). This bone segmentation was projected (p_2) and combined with the original acquisition (p_0) to compute the products p_0p_2 and p_2^2. These products were reconstructed, obtaining the basis images f_0, f_{01}, f_{11} and f_{02}, which were linearly combined according to:

$$f_c = f_0 + c_{01}f_{01} + c_{11}f_{11} + c_{02}f_{02}, \tag{7}$$

where f_c is the corrected image and the weights c_{ij} were automatically calculated by minimizing the total variation of f_c with the simplex algorithm. Initial weights of the algorithm c_{01}, c_{11} and c_{02} were set to 0, 0 and 0.1 for the simulated data and to 0, 0 and 0 for the real data.

For the sfEBHC method, values above the threshold $f_{LOW} = 0$ in the initial reconstruction were increased based on a non-linear transformation controlled by parameter $\eta = 0.001$ (all values were extracted from Schuller *et al* (2015)). The transformed reconstruction was projected (q) and combined with the original acquisition (p) into nine monomials, p^iq^j, with $0 \leqslant i, j \leqslant 2$. These monomials were reconstructed (f_{ij}) and linearly combined according to

$$f_c = f_{10} + {\sum_{ij}}' c_{ij}f_{ij}, \tag{8}$$

where f_c is the corrected image and c_{ij} the weights, which were automatically calculated by minimizing the entropy of f_c and initially set to 0 and 0.05 for simulated and real data, respectively. The primed sum indicates that f_{00}, f_{10} and f_{01} are excluded from the linear combination.

JS_{pol}, EBHC and sfEBHC were evaluated with the different options for the prior water-linearization step: using both ideal (soft tissue) and realistic (PMMA) half-cylinder calibration phantoms for simulations, and the half-cylinder phantom made of PMMA (figure 5, top row) for real data.

The calibration needed in 2DCalBH was evaluated with a phantom made up of a half cylinder of soft-tissue equivalent material (radius of 3 cm) plus one triangular prism with rounded corners of bone equivalent material (height of 2.5 cm and width of 6 cm). This design enables simultaneous measurement of different combinations of soft tissue and bone as found in preclinical studies. We tested two approaches: (1) a digital phantom

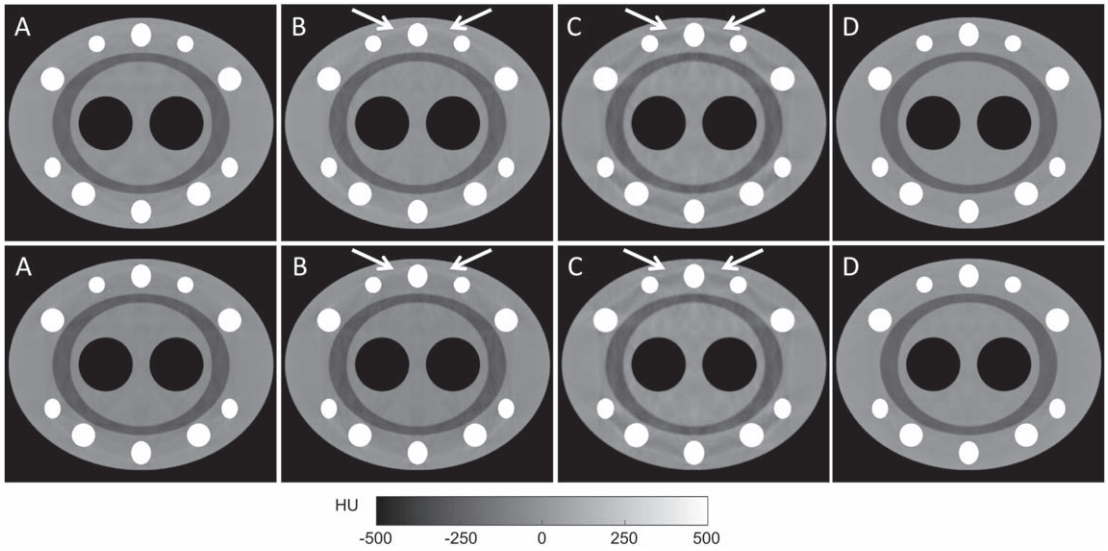

Figure 6. Preclinical evaluation phantom for the 50 kVp polychromatic acquisition corrected with JS_{pol} (A), EBHC (B), sfEBHC (C) and 2DCalBH (D) using the ideal (top row) and realistic (bottom row) calibration phantoms. Visualization of these images with a narrower window width can be found in the supplementary data.

Table 4. RMSE of the preclinical evaluation phantom with respect to the monochromatic reconstruction for the 40 and 50 kVp scenarios (HU).

			JS_{pol}		EBHC		sfEBHC		2DCalBH	
kVp	ROI	No correction	Ideal (ST)	Realistic (PMMA)	Ideal (ST)	Realistic (PMMA)	Ideal (ST)	Realistic (PMMA)	Ideal (ST-Bone)	Realistic (PMMA-AL6082)
40	Whole image	525.4	22.6	33.3	250.6	285.9	228.9	270.5	23.6	31.8
	ST	105.3	24.9	38.6	26.1	38.5	50.5	40.9	27.5	37.3
	Bone	2113.6	32.3	38.8	1018.6	1159.1	917.0	1094.3	24.0	28.0
50	Whole image	489.2	20.8	33.3	247.7	297.39	287.5	270.5	21.6	31.0
	ST	98.2	22.8	38.6	24.2	42.04	40.1	40.9	23.9	36.7
	Bone	1976.1	32.6	38.8	1011.5	1210.01	1169.1	1094.3	33.7	21.6

composed of soft tissue and bone (ideal), used for simulations and (2) digital and true phantoms composed of PMMA and AL6082 (realistic) for simulations and real data respectively (figure 5, bottom row). The phantom was acquired without the scanner bed, so the beam-hardening effect depends only on the two equivalent materials.

4. Results

4.1. Simulated data

Table 4 shows the RMSE with respect to the monochromatic reconstruction for all the methods and the different preclinical scenarios. Figure 6 shows the images reconstructed with each method for the 50 kVp acquisition (similar visual results were obtained at 40 kVp). JS_{pol} corrected both cupping and dark bands with both calibration phantoms, but using the realistic phantom increased the RMSE by 50% with respect to using the ideal one. EBHC increased the RMSE in soft tissue by 8% with respect to JS_{pol} with the ideal phantom, which can be seen in the worst compensation of the dark bands indicated with white arrows in figure 6(B). sfEBHC was the method with the worst dark-band correction, further increasing the error in soft tissue by 66% with respect to EBHC (see white arrows in figure 6(C)). Neither EBHC nor sfEBHC were able to recover monochromatic bone values, with errors above 900 HU. The proposed method showed an RMSE and a visual correction (figure 6(D)) similar to the JS_{pol} method independently of the calibration phantom.

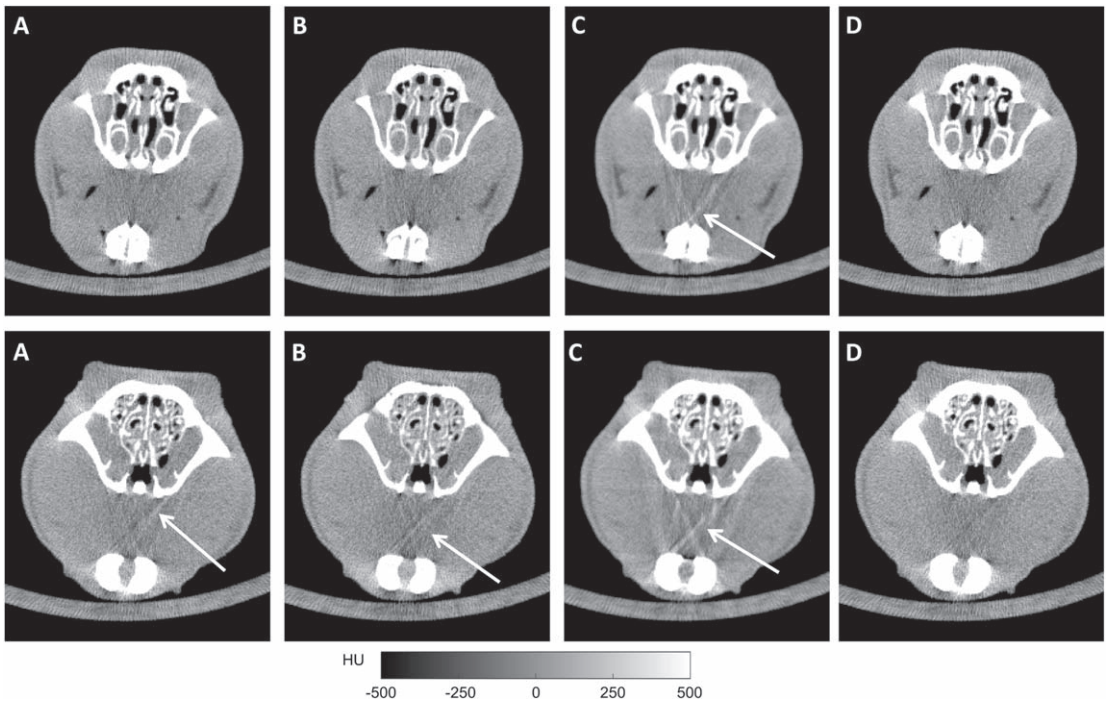

Figure 7. Axial slice to find the parameters of the JS_{pol} method (top row) and a second slice (bottom row) of the head study at 50 kVp corrected with JS_{pol} (A), EBHC (B), sfEBHC (C), and 2DCalBH (D). White arrows indicate dark-band artifacts. Visualization of the images with narrower window-width can be found in the supplementary data.

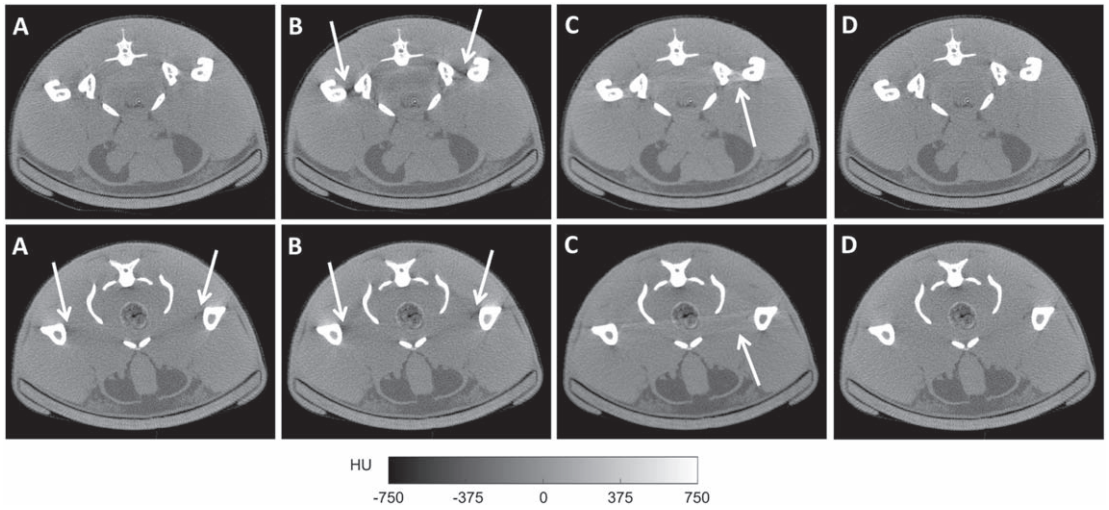

Figure 8. Axial slice to find the parameters of the JS_{pol} method (top row) and second slice (bottom row) of the abdominal study at 50 kVp corrected with JS_{pol} (A), EBHC (B), sfEBHC (C), and 2DCalBH (D). White arrows indicate dark-band artifacts. Visualization of these images with narrower window width can be found in the supplementary data.

4.2. Real data

Figures 7 and 8 show the results from head and abdominal rodent studies in the 50 kVp scenario (similar results were obtained for 40 kVp). Similar to simulated data, the JS_{pol} method properly corrected the dark bands in the slice used to optimize the parameters but did not completely compensate them in the other slice (see white arrows in figures 7(A) and 8(A)). EBHC showed a good compensation of the dark bands in one slice of the head study but an undercorrection in the other slice of the head study and the abdominal study (see white arrows in figures 7(B) and 8(B)). sfEBHC showed an overcorrection of both slices of the abdominal and head studies indicated by white arrows in figures 7(C) and 8(C). The proposed method, 2DCalBH, presented a good correction in all slices of the head and abdominal studies.

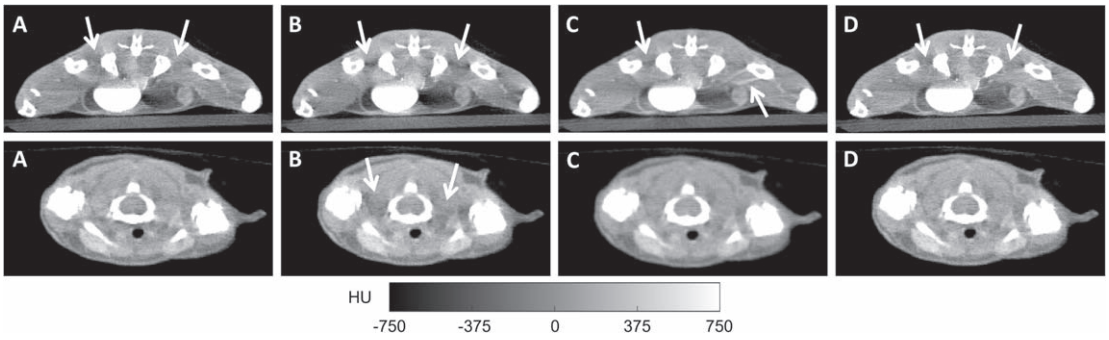

Figure 9. Axial slice with contrast agent (top row) and a second slice (bottom row) of the mouse study at 50 kVp corrected with JS_{pol} (A), EBHC (B), sfEBHC (C), and 2DCalBH (D). White arrows indicate dark-band artifacts.

Figure 9 shows the results for the contrast-enhanced mouse study. As in the abdominal study, EBHC was not able to eliminate the dark bands independently of the bone thickness or the presence of contrast agent. sfEBHC produced a good compensation of the dark bands in slices with no contrast agent but an undercorrection between bones and an overcorrection between bone and the bladder filled with contrast agent (see white arrows in figure 9(C)). JS_{pol} and 2DCalBH showed a good dark-band compensation in the slices with no contrast agent but only reduced them in the slices with contrast agent.

5. Discussion and conclusions

This work presents a new beam hardening correction method for CT that extends the water linearization to correct both cupping and dark-band artifacts. The proposed method is based on characterizing the polychromatic attenuation of the tissues and their corresponding monochromatic attenuation values through a calibration with a simple phantom made up of soft-tissue and bone equivalent materials. This calibration is similar to that already needed in most of the previous post-processing methods that include a prior water linearization step. The proposed approach has a similar basis to the method proposed by Joseph *et al* (1978) with the main difference being in the way to estimate the beam hardening effect: Joseph *et al* analytically approximate this effect with the knowledge of the spectrum and the mass attenuation coefficients of the tissues, while 2DCalBH uses a calibration step to eliminate the need for this knowledge.

We evaluated our method against one classical beam hardening correction method (JS_{pol}) and two of the latest post-processing methods found in the literature, EBHC (Kyriakou *et al* 2010) and sfEBHC (Kyriakou *et al* 2010).

Evaluation on simulated data showed that in soft tissue EBHC had errors similar to those of the proposed method while sfEBHC doubled the error. In bone, both EBHC and sfEBHC showed the highest errors of the compared methods, thus hindering the recovery of monochromatic bone values. Results of EBHC on real data showed a good correction in the head study but an undercorrection in the abdominal and contrast-enhanced studies. An undercorrection with EBHC had been previously shown by Jin, *et al* (2015) in simulated data. Similarly, results of sfEBHC on real data showed a certain overcorrection of the rodent studies, in agreement with the evaluation presented by Schuller *et al* (2015).

The errors yielded by JS_{pol} and the proposed method are similar for simulated data. However, this comparison is unrealistic as the coefficients of the JS_{pol} method were obtained by taking into account the ideal attenuation values that are unavailable in real data. In the latter case, JS_{pol} coefficients were obtained by visual inspection of one representative slice of each study, since no unique set of parameters resulted in a proper correction of all the slices within a volume. This might be due to the limitations of the two-parameter model employed in the JS_{pol} method, which may not be able to fully characterize different combinations of soft-tissue and bone thicknesses. In contrast, the proposed method generates a correction factor for all possible soft-tissue and bone combinations, resulting in a proper compensation of the dark bands in all cases.

Evaluation on the contrast-enhanced mouse study showed that the assumption of the soft-tissue and bone model was not completely accurate when not only bone and soft tissue are present. It would be interesting to study a model with three materials, which would need a more complex phantom having an extra material with the attenuation properties of the contrast agent. Since bone and iodine have similar reconstructed values, a simple threshold may be insufficient to separate both, being necessary to use other approaches, such as dynamic segmentation (Stenner *et al* 2010). Same strategy could by applied in case of a metallic implant.

The main limitation of the proposed method, shared by most previous post-processing methods, is the need of a preliminary bone segmentation. Errors in this bone segmentation may hinder the selection of the appropriate linearization functions, which could lead to inconsistent data in the corrected projection values. Future work will evaluate the integration of the presented beam-hardening model into the projection matrix of an iterative method, as in Abella *et al* (2020), to cope with low-dose data. Although simulations were done with an ideal detector and no scatter contribution, results in real data showed a good visual artifact correction. Nevertheless, future work will study if these effects hinder the quantification. Also, although PMMA and aluminum have been previously used as soft-tissue and bone equivalent materials (Brody *et al* 1981, Lehmann *et al* 1981), it would be interesting to explore the impact of more sophisticated equivalent materials (White *et al* 1977, Goodsitt 1992, Jones *et al* 2003) on image quantification.

The focus of this work is small-animal imaging. Nevertheless, we expect the proposed method to also work in clinical scenarios, provided that the size of the calibration phantom is optimized to fit bone and soft-tissue thicknesses in the human body, the geometry is adapted in the projection kernel and the scatter effect is evaluated, as it is more important in clinical studies.

A key advantage of the proposed method is that the calibration needs only a small modification over the standard method already available in most commercial scanners, easing its incorporation into the workflow without requiring changes in the acquisition and reconstruction stages or in the system hardware.

Acknowledgments

This work has been supported by Ministerio de Ciencia e Innovación, Agencia Estatal de Investigación: DPI2016-79075-R - AEI/FEDER, UE, co funded by European Regional Development Fund, 'A way of making Europe'; PDC2021-121656-I00 (MULTIRAD), funded by MCIN/AEI/10.13039/501100011033 and by the European Union 'NextGenerationEU'/PRTR; PID2019-110369RB-I00/AEI/10.13039/501100011033 (RADHOR). Also funded by Comunidad de Madrid: Multiannual Agreement with UC3M in the line of 'Fostering Young Doctors Research' (DEEPCT-CM-UC3M), and in the context of the V PRICIT (Regional Programme of Research and Technological Innovation"); S2017/BMD-3867 RENIM-CM, co-funded by European Structural and Investment Fund. And also partially funded by CRUE Universidades, CSIC and Banco Santander (Fondo Supera Covid19), project RADCOV19. The CNIC is supported by Instituto de Salud Carlos III, Ministerio de Ciencia e Innovación and the Pro CNIC Foundation.

References

Abella M, Serrano E, Garcia-Blas J, Garcia I, de Molina C, Carretero J and Desco M 2017 FUX-Sim: implementation of a fast universal simulation/reconstruction framework for x-ray systems *PLoS One* **12** 1–22

Abella M, Martinez C, Desco M, Vaquero J J and Fessler J A 2020 Simplified statistical image reconstruction for x-ray ct with beam-hardening artifact compensation *IEEE Trans. Med. Imaging* **39** 111–8

Alvarez R E and Macovski A 1976 Energy-selective reconstructions in x-ray computerised tomography *Phys. Med. Biol.* **21** 733–44

Brody W R, Butt G, Hall A and Macovski A 1981 A method for selective tissue and bone visualization using dual energy scanned projection radiography *Med. Phys.* **8** 353–7

Brooks R A and Di Chiro G 1976 Beam hardening in x-ray reconstructive tomography *Phys. Med. Biol.* **21** 390–8

De Man B, Nuyts J, Dupont P, Marchal G and Suetens P 2001 An iterative maximum-likelihood polychromatic algorithm for CT *IEEE Trans. Med. Imaging* **20** 999–1008

Elbakri I A and Fessler J A 2003 Segmentation-free statistical image reconstruction for polyenergetic x-ray computed tomography with experimental validation *Phys. Med. Biol.* **48** 2453–77

Elbakri I A and Fessler J A 2002 Statistical image reconstruction for polyenergetic x-ray computed tomography *IEEE Trans. Med. Imaging* **21** 89–99

Feldkamp L A, Davis L C and Kress J W 1984 Practical cone-beam algorithm *J. Opt. Soc. Am.* A **1** 612–9

Goodsitt M M 1992 Evaluation of a new set of calibration standards for the measurement of fat content via DPA and DXA *Med. Phys.* **19** 35–44

Herman G T 1979 Correction for beam hardening in computed tomography *Phys. Med. Biol.* **24** 81–106

Hubbell J H and Seltzer S M 1995 Tables of x-ray mass attenuation coefficients and mass energy-absorption coefficients 1 keV to 20 meV for elements z = 1 to 92 and 48 additional substances of dosimetric interest *NIST Standard Reference Database 126* NISTIR-5632TRN: 51812148 Radiation Physics Division, PML, NIST (https://doi.org/10.18434/T4D01F)

Jin P, Bouman C A and Sauer K D 2015 A model-based image reconstruction algorithm with simultaneous beam hardening correction for x-ray CT *IEEE Trans. Comput. Imaging* **1** 200–16

Jones A K, Hintenlang D and Bolch W 2003 Tissue-equivalent materials for construction of tomographic dosimetry phantoms in pediatric radiology *Med. Phys.* **30** 2072–81

Joseph P M and Spital R D 1978 A method for correcting bone induced artifacts in computed tomography scanners *J. Comput. Assist. Tomogr.* **2** 100–8

Kyriakou Y, Meyer E, Prell D and Kachelriess M 2010 Empirical beam hardening correction (EBHC) for CT *Med. Phys.* **37** 5179–87

Lehmann L *et al* 1981 Generalized image combinations in dual KVP digital radiography *Med. Phys.* **8** 659–67

Martínez C, De Molina C, Desco M and Abella M 2016 Simple method for beam-hardening correction based on a 2D linearization function *Paper presented at: The 4th Int. Meeting on Image Formation in x-ray Computed Tomography (CTMeeting 2016)* (Bamberg)

Martinez C, de Molina C, Desco M and Abella M 2020 Optimization of a calibration phantom for quantitative radiography *Med. Phys.* **48** 1039–53
Nalcioglu O and Lou R Y 1979 Post-reconstruction method for beam hardening in computerised tomography *Phys. Med. Biol.* **24** 330–340
Schuller S *et al* 2015 Segmentation-free empirical beam hardening correction for CT *Med. Phys.* **42** 794–803
Stenner P, Schmidt B, Allmendinger T, Flohr T and Kachelrie M 2010 Dynamic iterative beam hardening correction (DIBHC) in myocardial perfusion imaging using contrast-enhanced computed tomography *Investigative Radiol.* **45** 314–23
Vaquero J J *et al* 2008 Assessment of a New High-performance small-animal x-ray tomograph *IEEE Trans. Nucl. Sci.* **55** 898–905
White D, Martin R and Darlison R 1977 Epoxy resin based tissue substitutes *Br. J. Radiol.* **50** 814–21
Würfl T 2020 *Applications of Data Consistency Conditions in Cone-Beam Computed Tomography* Friedrich-Alexander-Universität Erlangen-Nürnberg (https://opus4.kobv.de/opus4-fau/frontdoor/index/index/docId/15426)
Würfl T, Hoffmann M, Aichert A, Maier A K, Maaß N and Dennerlein F 2019 Calibration-free beam hardening reduction in x-ray CBCT using the epipolar consistency condition and physical constraints *Med. Phys.* **46** e810–22
Yan C H, Whalen R T, Beaupre G S, Yen S Y and Napel S 2000 Reconstruction algorithm for polychromatic CT imaging: application to beam hardening correction *IEEE Trans. Med. Imaging* **19** 1–11

This document contains the supplementary data of the manuscript: “Simple Beam-Hardening Correction Method (2DCalBH) based on 2D linearization” by C. Martinez, J. A. Fessler, M. Desco and M. Abella. We provide figures of simulated and real data with a reduced window width to better appreciate the correction of the dark bands, an extra plot to support the selection of equivalent materials, and results of two extra simulated experiments based on the phantoms found in Kyriakou et al. (EBHC) and Schuller et al. (sfEBHC) for a comprehensive comparison with those methods.

Narrower window

The following figures replicate Figures 3 and 6 of the manuscript, showing the reconstruction of simulated monochromatic and polychromatic data with a reduced window-width. Although this window-width is not usually used in preclinical research, we show it here to better appreciate the correction of the dark bands. As we can see in Figure 6-B, although none of the methods was able to completely eliminate the dark bands among the bones in simulated data, JSpol and 2DCalBH are the ones with better compensation, while 2DCalBH showed the best correction in the inner ellipse.

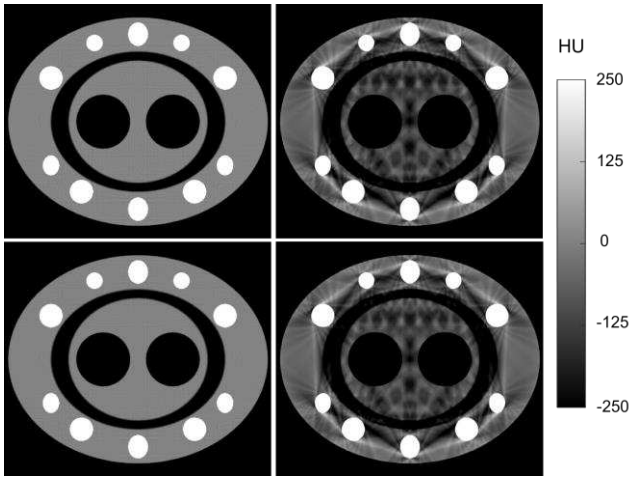

Figure 3-B. Preclinical evaluation phantom using monochromatic (left) and polychromatic (right) simulations at 40 kVp (top) and 50 kVp (bottom), reconstructed using the FBP algorithm.

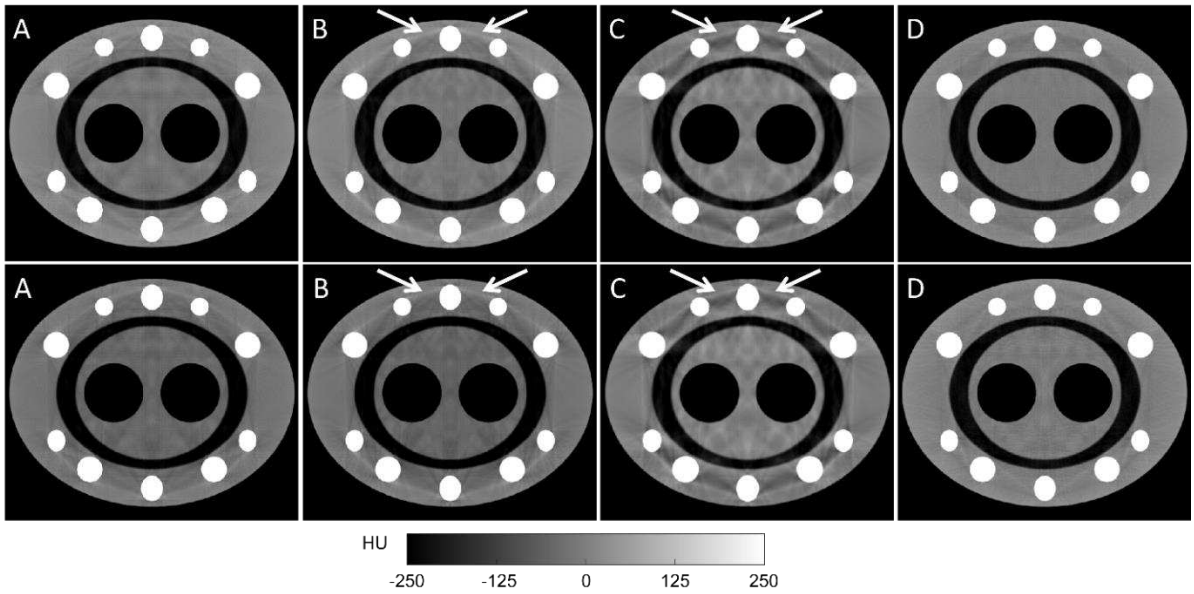

Figure 6-B. Preclinical evaluation phantom for the 50 kVp polychromatic acquisition corrected with JSpol (A), EBHC (B), sfEBHC (C) and 2DCalBH (D) using the ideal (top) and realistic (bottom) calibration phantoms.

Figures 4-B, 7-B, 8-B and 9-B show the same slices of the head and abdomen of the rat and the mouse than Figures 4, 7, 8 and 9 of the submitted manuscript but with a narrower window width to further highlight the dark bands. Again, even though part of the dark bands are still present after correction, 2DCalBH is the method that results in the best compensation.

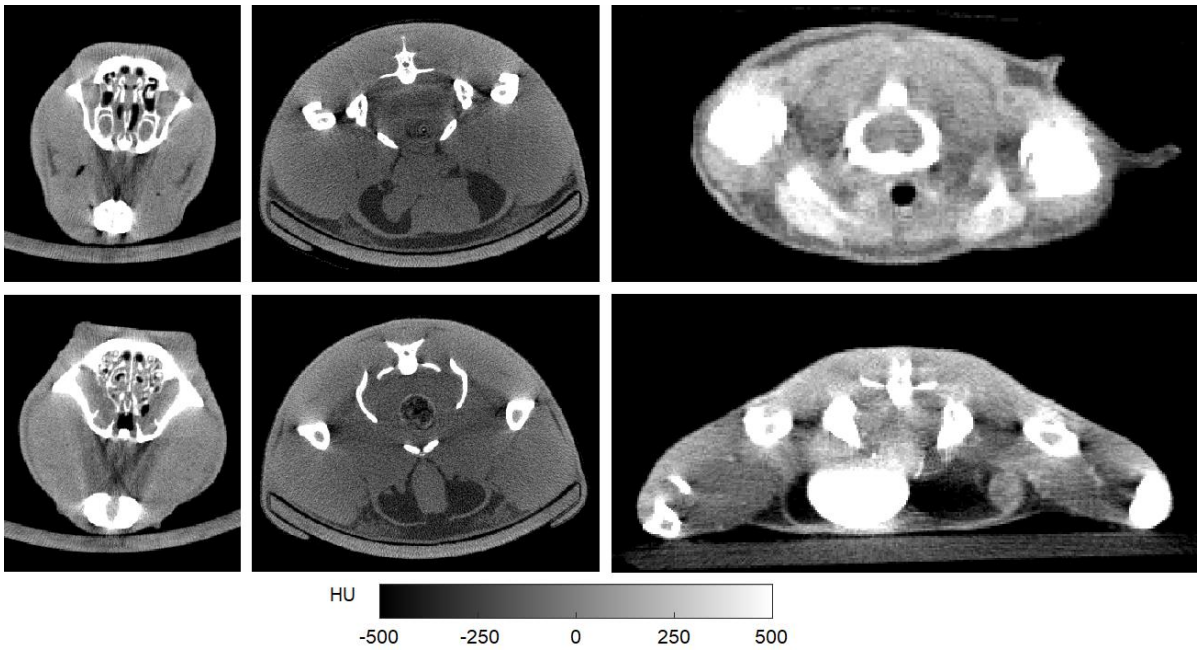

Figure 4-B. Axial slices used to optimize the JSpol coefficients (top) and a second slice of the same study (bottom) for the rat head (left) and abdomen (center) studies at 50 kVp and the contrast-enhanced mouse study (right) at 40 kVp, reconstructed using the FDK algorithm.

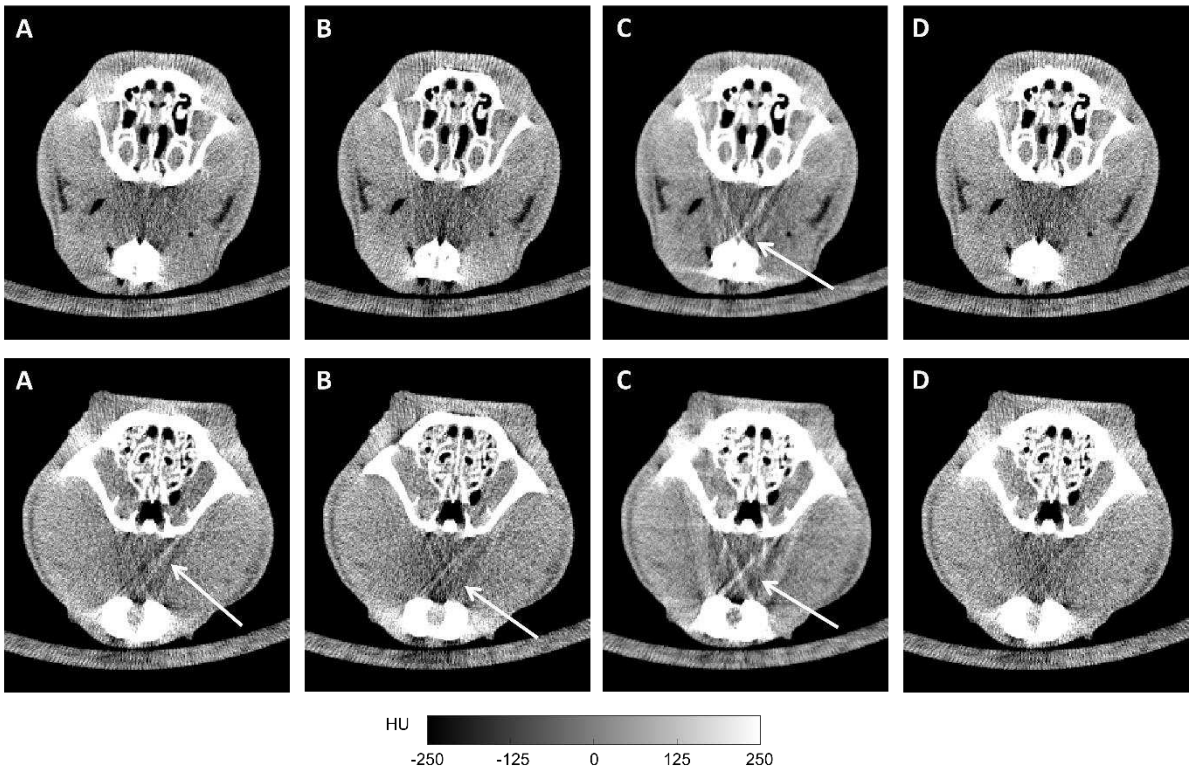

Figure 7-B. Axial slice to find the parameters of the JSpol method (top) and a second slice (bottom) of the head study at 50 kVp corrected with JSpol (A), EBHC (B), sfEBHC (C), and 2DCalBH (D). Arrows indicate dark-band artifacts.

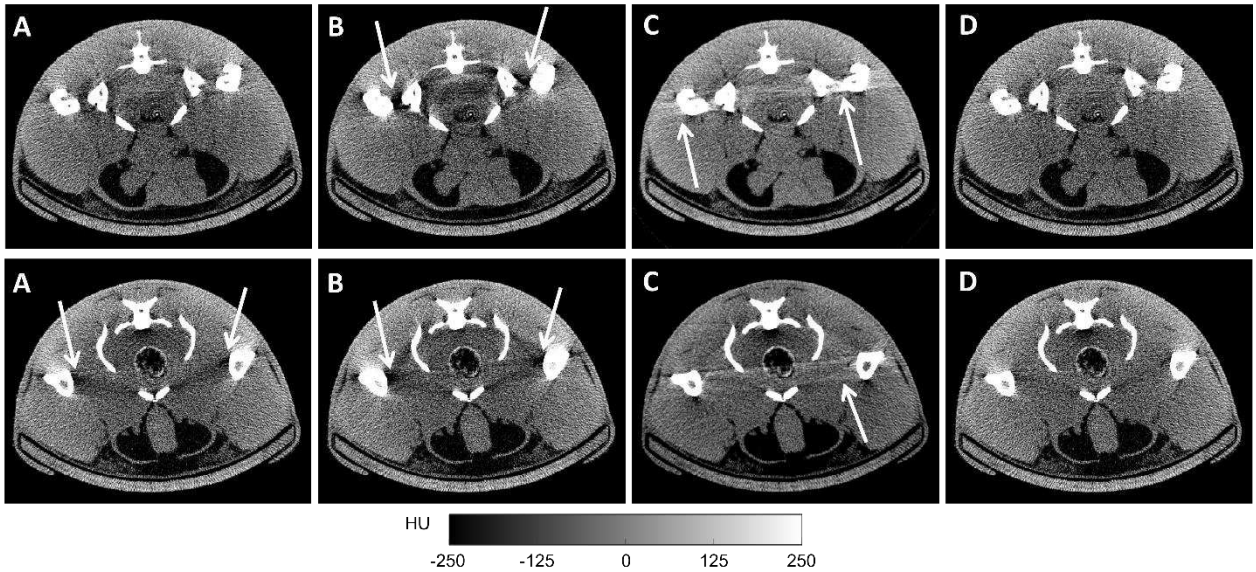

Figure 8-B. Axial slice to find the parameters of the JSpol method (top) and second slice (bottom) of the abdominal study at 50 kVp corrected with JSpol (A), EBHC (B), sfEBHC (C), and 2DCalBH (D). White arrows indicate dark-band artifacts.

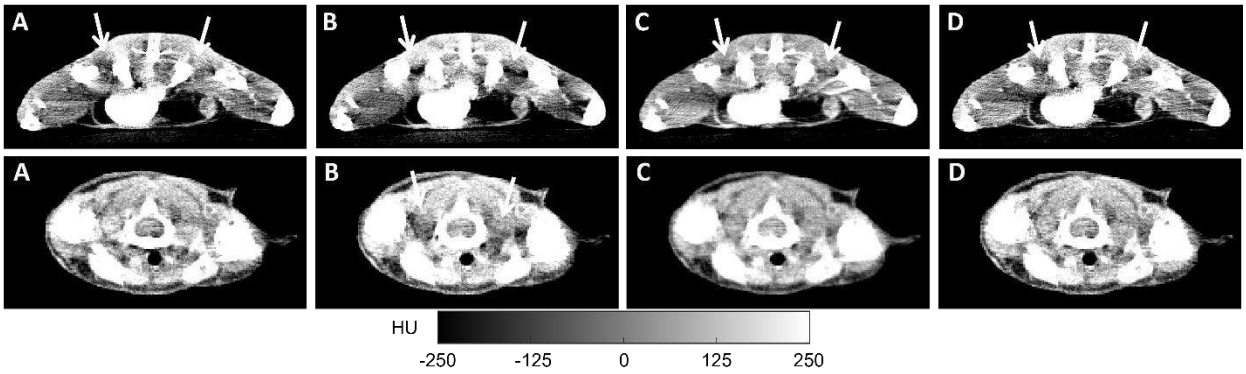

Figure 9-B. Axial slice with contrast agent (top) and a second slice (bottom) of the head study at 50 kVp corrected with JSpol (A), EBHC (B), sfEBHC (C), and 2DCalBH (D). Arrows indicate dark-band artifacts.

Equivalent materials

While PMMA is a good substitute for soft tissue in terms of beam-hardening effect, as shown in the left panel of Figure 1-E, AL6082 does not completely match bone in this regard. The deviation we can see in the right panel of Figure 1-E is due to the difference in density between cortical bone (1.92 g/cm3) and AL6082 (2.7 g/cm3). This is compensated by multiplying the bone thickness by a weighting factor equal to the ratio of densities, 2.7/1.92.

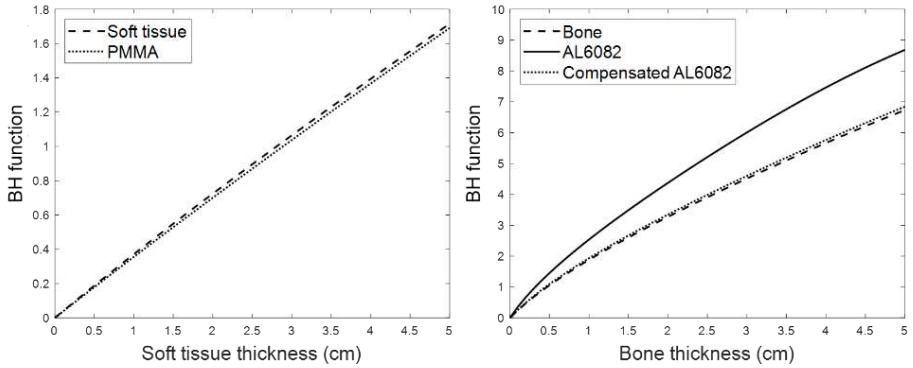

Figure 1-E. Beam-hardening function of the soft tissue and PMMA (left); and of the bone, AL6082 before and after compensation (right). Beam-hardening functions were simulated with a 50 kVp spectrum.

Extra experiments – simulated data

Figures 2-E and 3-E show the reconstruction of the phantom similar to the one used in the Kyriakou et al.[1] manuscript (EBHC) but adapted to a small animal scanner. It was made up of a soft-tissue ellipse (1 g/cm^3) with 5 cm diameter and three bone inserts (1.92 g/cm3) with 0.68 cm diameter. Mass attenuation coefficients and densities were obtained from the National Institute of Standards and Technology (NIST). Projection data were simulated with the MIRT toolbox (http://web.eecs.umich.edu/~fessler/code/index.html), based on parallel-beam geometry, generating 360 projections within a 360 degrees angular span, with a source of 50 kVp.

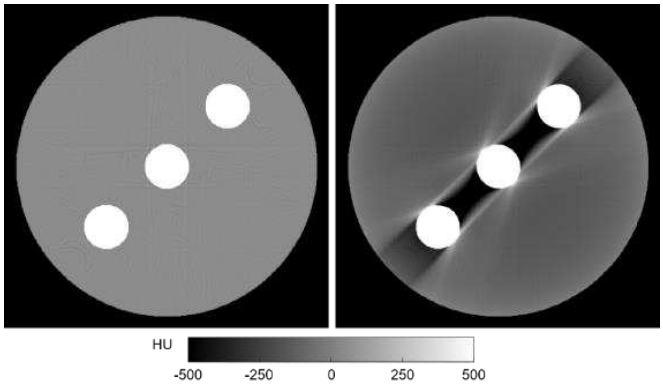

Figure 2-E. Monochromatic and polychromatic reconstruction of the phantom used by Kyriakou et al.[1] adapted to a small-animal scenario.

We did not find any set of optimal parameters to completely eliminate the dark bands with JSpol, which showed a similar undercompensation to EBHC. In contrast, sfEBHC and 2DCalBH showed a good artifact compensation in this case.

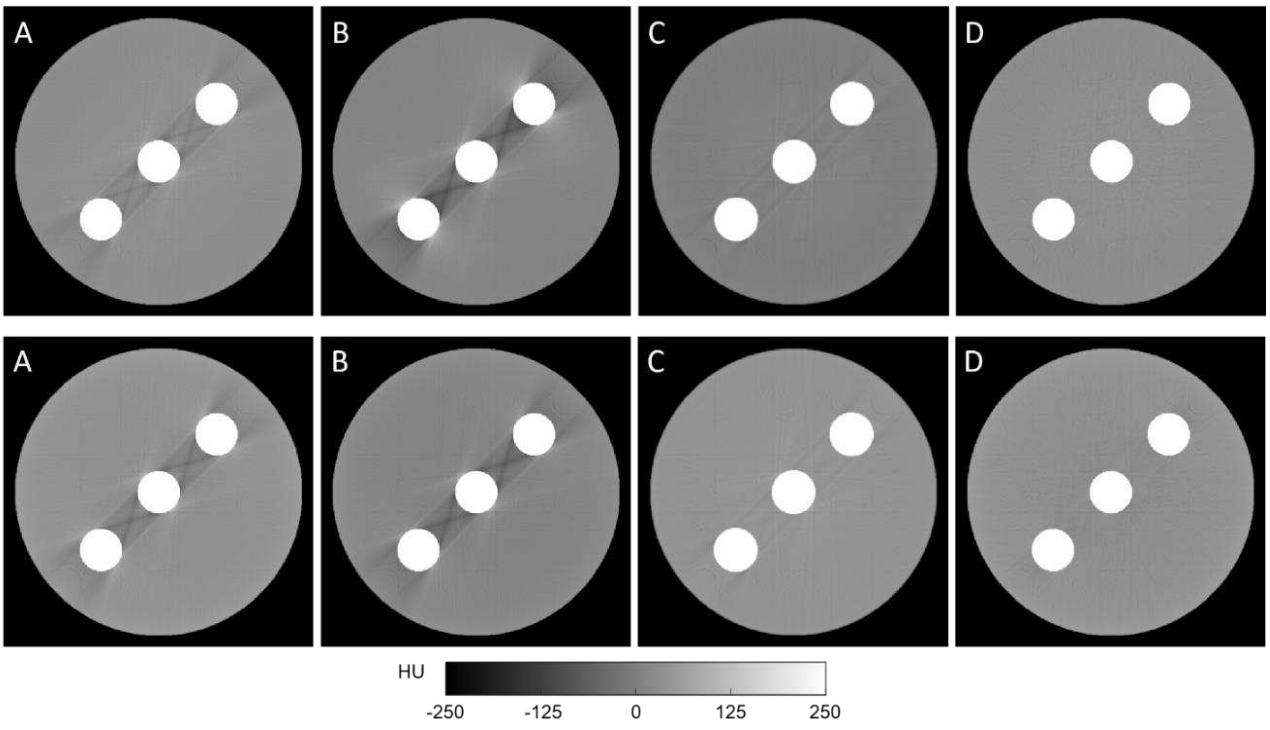

Figure 3-E. Small-animal adaptation of the phantom used by Kyriakou et al.[1] corrected with JSpol (A), EBHC (B), sfEBHC (C) and 2DCalBH (D) using the ideal (top) and realistic (bottom) calibration phantoms.

Figures 4-E and 5-E show the reconstruction of a small animal phantom similar to the one used by Schuller et al.[2] (sfEBHC), also adapted to a small-animal scanner. It was made up of a soft-tissue ellipse (1 g/cm^3) with 5 cm of diameter, three bone inserts (1.92 g/cm^3) with 0.68 cm of diameter and a low-contrast water insert (1.05 g/cm^3) with 0.68 cm of diameter. Mass attenuation coefficient and densities for those materials were obtained from the National Institute of Standards and Technology (NIST). Projection data were simulated with the MIRT toolbox (http://web.eecs.umich.edu/~fessler/code/index.html), based on parallel-beam geometry, generating 360 projections within a 360 degrees angular span with a source voltage of 50 kVp.

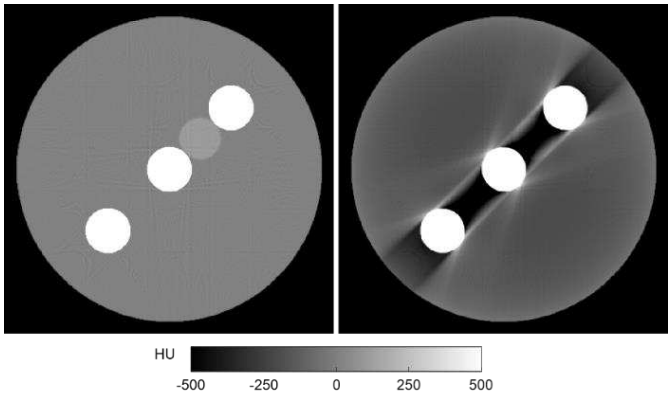

Figure 4-E. Monochromatic and polychromatic reconstruction of a small-animal adaptation of the phantom used by Schuller et al. [2]

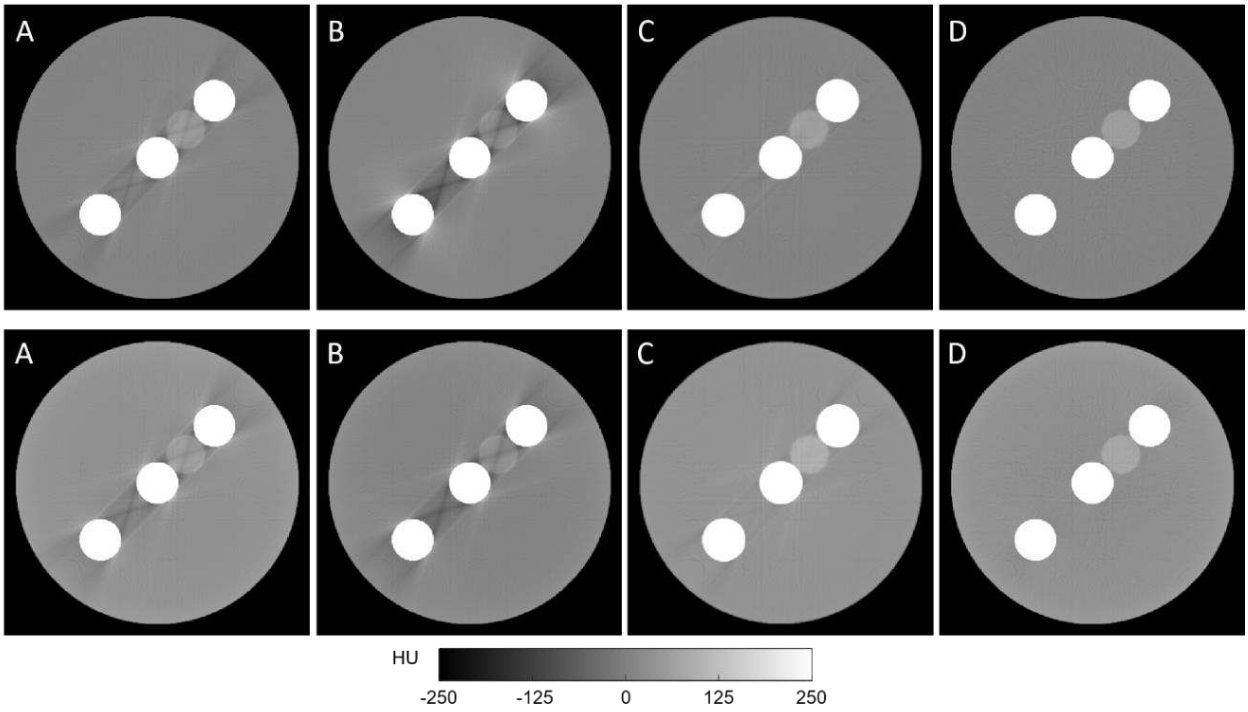

Figure 5-E. Small-animal adaptation of the phantom used by Schuller et al.2 corrected with JSpol (A), EBHC (B), sfEBHC (C) and 2DCalBH (D) using the ideal (top) and realistic (bottom) calibration phantoms. White arrows indicate a wrong correction of the artifacts.

We can see that the low-contrast water insert is completely hidden by the dark bands in the FBP polychromatic reconstruction, while all correction methods recovered it. Similar to the previous experiment, neither JSpol nor EBHC were able to completely eliminate the artifacts. sfEBHC and 2DCalBH were both able to reduce the dark bands, with 2DCalBH showing a slightly better result. Furthermore, the

performance of sfEBHC was worst on realistic samples, as the more complex phantom or the real rodent studies in the manuscript showed.

Extra experiments – real data

To add variability to our real data experiments and determine whether our good results are significant, we further evaluated the proposed method with two extra rodent studies, acquired with the CT subsystem of ARGUS PET/CT (SEDECAL). Acquisition parameters were 40 kVp and 340 µA, obtaining 360 projections of 514×574 pixels with a pixel size of 0.2 mm over 360 degrees angular span. Figures 6-E and 7-E show two different slices of each extra rodent study with FDK reconstruction before (top) and after (bottom) correction with 2DCalBH. 2DCalBH shows a good compensation of the dark bands independently of the bone distribution.

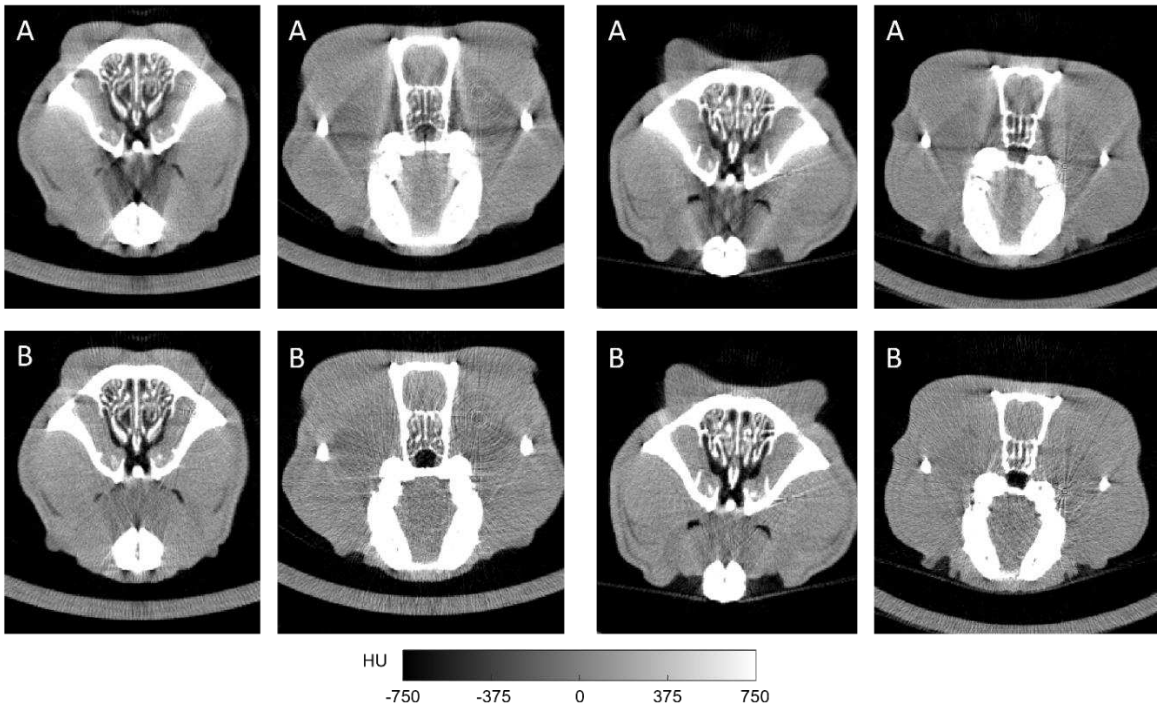

Figure 6-E. Axial slices of the FDK reconstruction (A) and corrected with 2DCalBH (B) of two extra rodent studies.

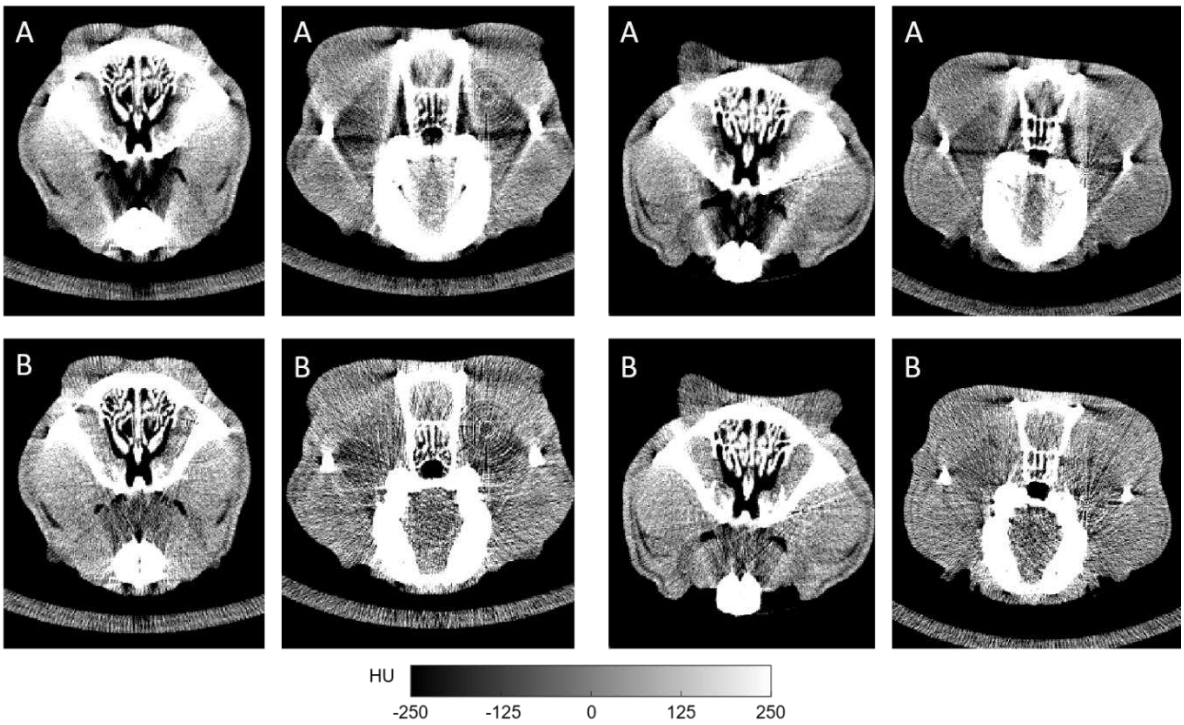

Figure 7-E. Axial slices of the FDK reconstruction (A) and corrected with 2DCalBH (B) of two extra rodent studies.

References

1. Kyriakou Y, Meyer E, Prell D, Kachelriess M. Empirical beam hardening correction (EBHC) for CT. *Medical physics.* Oct 2010;37(10):5179-5187.

2. Schuller S, Sawall S, Stannigel K, et al. Segmentation-free empirical beam hardening correction for CT. *Medical physics.* Feb 2015;42(2):794-803.